SwRI GEMS Workshop

sc-CO2 as Working Fluid

11/19/2024

Prof. Mayank Tyagi

Louisiana State University

mtyagi@lsu.edu

Opportunities to collaborate with Academia

- Well Control
- Testing Surface/Downhole Equipment.
- Training/Workshops

...

LSU to drill carbon capture research well on campus

BY: **PIPER HUTCHINSON** - MARCH 22, 2024 11:50 AM

LSU's Petroleum Engineering Research, Training and Testing Lab (LSU Engineering photo)

LSU's College of Engineering will soon drill a new well on campus to research carbon capture, utilization and storage (CCUS).

The well will be added to LSU's Petroleum Engineering Research, Training and Testing Lab, a hands-on research facility near Alex Box Stadium made up of two industrial-scale research wells, additional storage wells and surface facilities.

CO_2 Phase Diagram and Power Cycles - Overview

Credit: Wikimedia Commons

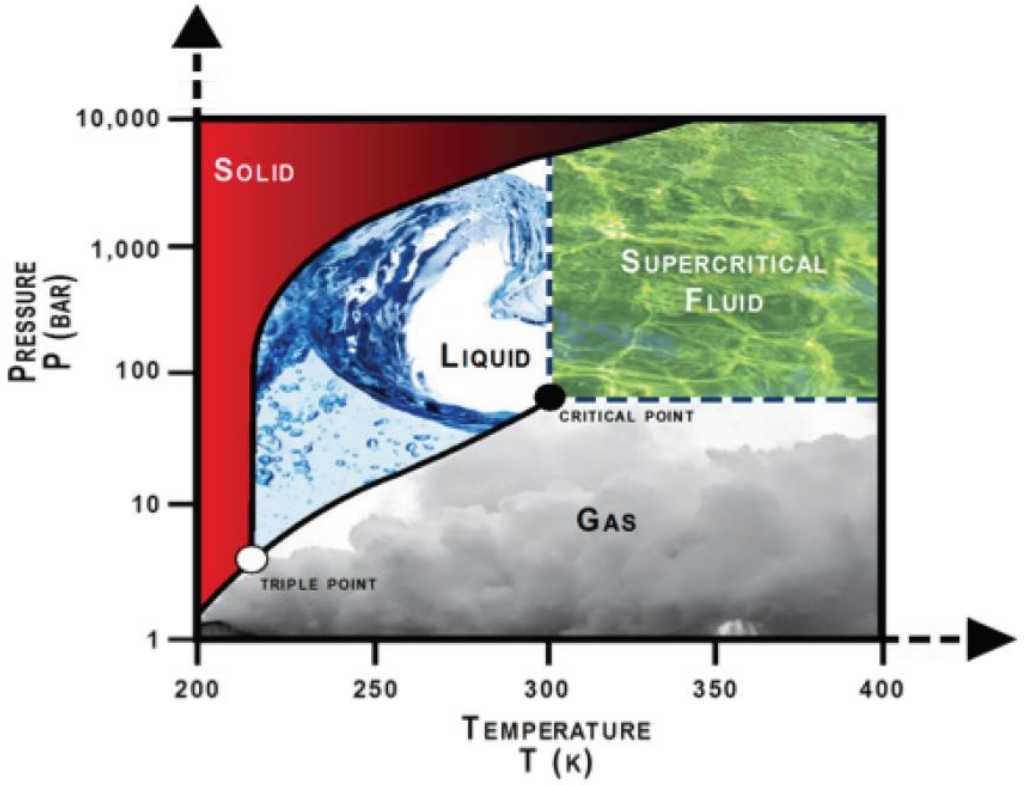

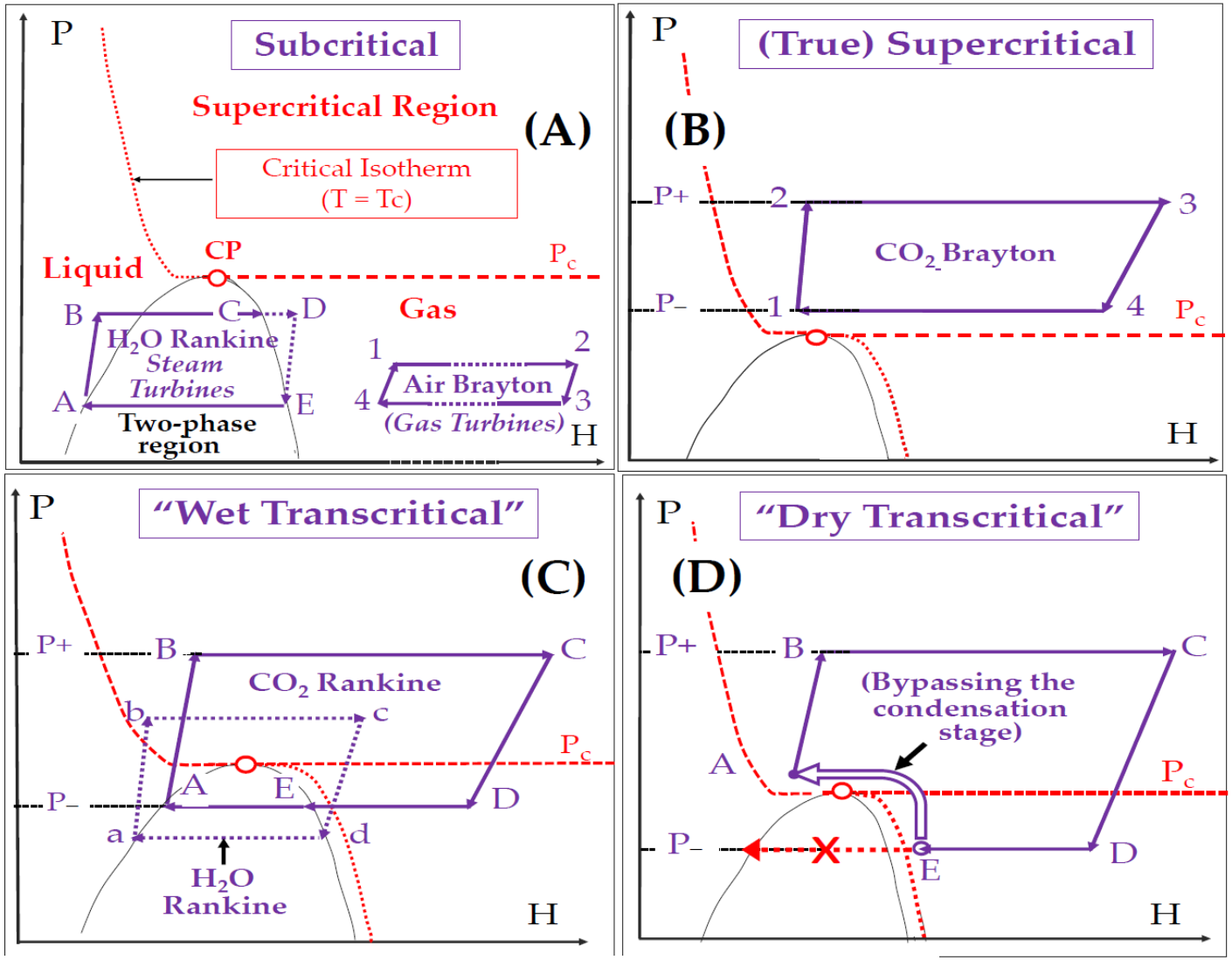

Article

Supercritical CO_2 Power Technology: Strengths but Challenges

Michel Molière [1,2,*], Romain Privat [1], Jean-Noël Jaubert [1] and Frédéric Geiger [3]

Energies **2024**, *17*, 1129. https://doi.org/10.3390/en17051129

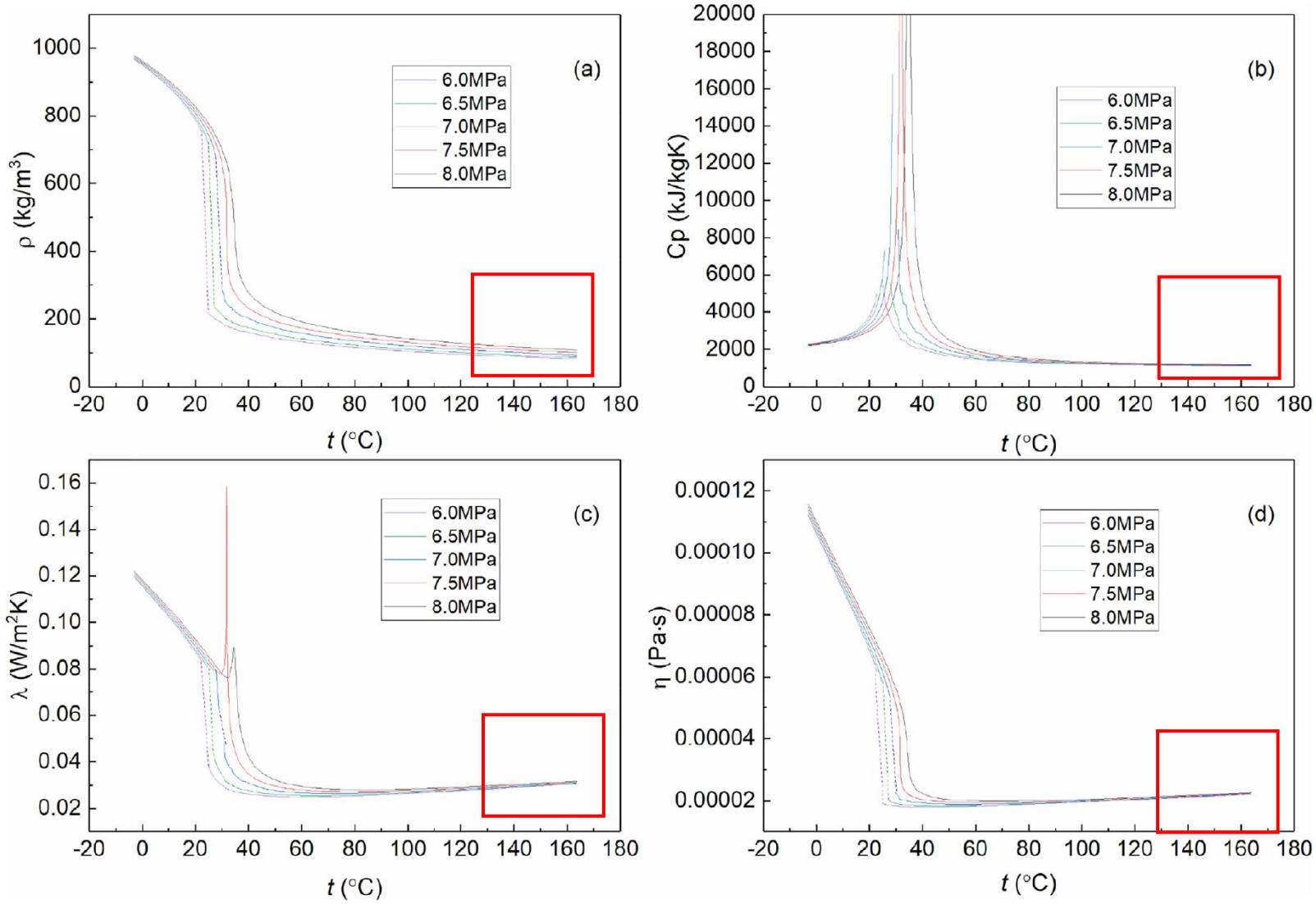

Fig. 1. Variation in thermophysical properties of CO_2 in the supercritical region at different pressures [12]: (a) density, (b) specific heat, (c) thermal conductivity, (d) viscosity.

Experimental comparison of the heat transfer of carbon dioxide under subcritical and supercritical pressures

International Journal of Heat and Mass Transfer 152 (2020) 119562

Xianliang Lei[a,*], Ruifeng Peng[a], Ziman Guo[a], Huixiong Li[a], Kashif Ali[a], Xu Zhou[b]

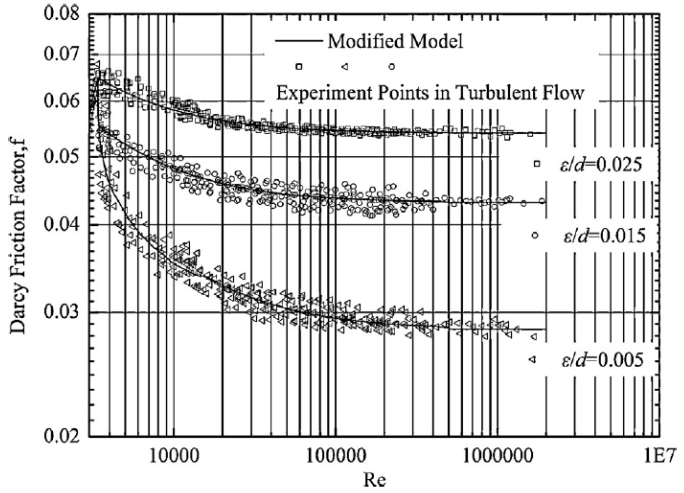

Fig. 15. Experimental data for friction coefficient of various roughness and calculation curve of Eq. (12).

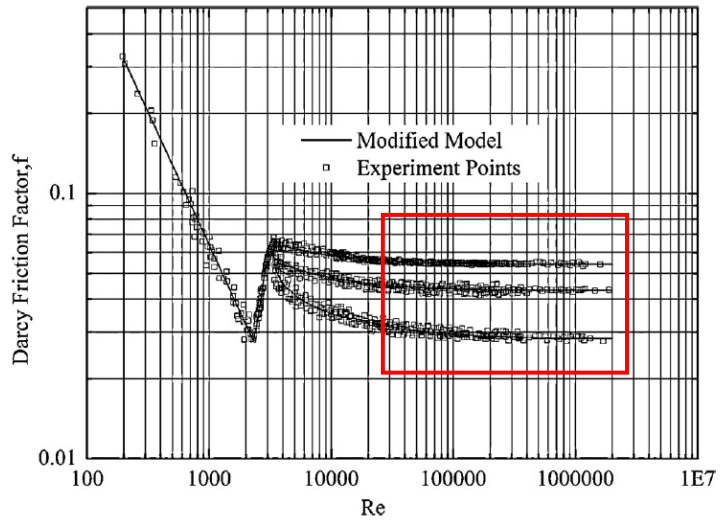

Fig. 16. Different experimental data points for friction coefficients with various Reynolds numbers and the calculation curve of Eq. (13).

(1) Temperature and pressure have impact on density and viscosity of SC-CO_2, furthermore, influence *Re*, making it change abruptly near the critical point. But Re can reflect variation of physical property parameter comprehensively, function $\lambda = f(Re)$ can still be used to determine the friction coefficient of SC-CO_2.

(2) The friction coefficient of SC-CO_2 in the laminar region is lowered as the Reynolds number increases, the experimental relationship between λ and *Re* corresponds with the relation in equation $\lambda = 64/Re$, with the relative average error −1.1%, absolute average error 2.39%.

(3) The friction coefficient of SC-CO_2 in the transition region increases as the Reynolds number does. Five relations of friction coefficient are compared with the experimental data. The absolute average errors of 5 formulae are high, and not suitable for calculating SC-CO_2 friction coefficient. Modified calculation model for SC-CO_2 friction coefficient in the transition region is set up by regression, of which the absolute average error is 2.81%.

(4) The friction coefficient of SC-CO_2 in the turbulent flow region is reduced as the Reynolds number increases, and it becomes flat at last. 15 relations of friction coefficient are compared with the experimental data, and calculation values are lower than the experimental data. Take formula Colebrook–White as a representative one, the error is bigger within low Reynolds region ($3400 < Re < 11{,}000$). According to experimental data, the modified model for calculation of friction coefficient in the turbulent flow region is proposed with the absolute average error 1.94%, which can apply in practice conveniently.

Experimental study on the friction coefficient of supercritical carbon dioxide in pipes

Zhiyuan Wang*, Baojiang Sun, Jintang Wang, Lei Hou

International Journal of Greenhouse Gas Control 25 (2014) 151–161

Frictional Pressure Loss as a function of flowrate and pipe diameter

$$\left(\frac{\Delta p}{\Delta L}\right)_f = f\frac{\rho V^2}{2D} \qquad V = \frac{Q}{A} = \frac{4Q}{\pi D^2} \qquad \therefore \left(\frac{\Delta p}{\Delta L}\right)_f = f\frac{\rho V^2}{2D} \sim \frac{Q^2}{D^5}$$

For same Reynolds' number (Halving the flowrate in half of the pipe diameter flow path), we can assume friction factor to be 0.03 for fully turbulent case.

Case A: ID ~ 12", 2Q

Case A pressure loss ~ 1/8 (Case B pressure loss)

If we choose to flow the double flowrate in one pipe for Case B

Case B: ID ~ 5.5", Q

Case A pressure loss ~ 1/32 (Case B pressure loss)

Therefore, it supports our design for flowing through large diameter pipe in the production well.

How to Select Turbomachinery

For Your Application

Barber Nichols

The Seven Variables Are:

1.	Q	=	Rate of Volume Flow	$\frac{L^3}{T}$
2.	H	=	Head Change Through Machine	$\frac{L^2}{T^2}$
3.	N	=	Rotational Speed	$\frac{1}{T}$
4.	D	=	Rotor Diameter	L
5.	ρ	=	Fluid Density	$\frac{M}{L^3}$
6.	μ	=	Absolute Fluid Viscosity	$\frac{M}{L \cdot T}$
7.	H_S	=	Net Positive Suction Head	$\frac{L^2}{T^2}$
	or			
	a*	=	Speed of Sound in Fluid	$\frac{L}{T}$

$$N_s = \frac{N \cdot Q_3^{1/2}}{H_{ad}^{3/4}} \qquad D_s = \frac{D \cdot H_{ad}^{1/4}}{Q_3^{1/2}}$$

N	=	Rotational Speed (rpm)
Q_3	=	Rotor Flow Rate (ft^3/sec)
H_{ad}	=	Adiabatic Head (ft)
D	=	Diameter (ft)

The Turbine Hydraulic Efficiency as Derived From the Momentum Equation is:

$$\eta_H = \frac{2 \cdot U}{C_0}\left[\psi_N \cdot \sqrt{1-\rho} \cdot \cos\alpha - \frac{U}{C_0} + \psi_R \cdot \cos\beta_3 \cdot \sqrt{\rho + \psi_N^2 \cdot (1-\rho) - \frac{2 \cdot U}{C_0} \cdot \psi_N \cdot \sqrt{1-\rho} \cdot \cos\alpha + \frac{U^2}{C_0^2}}\right]$$

Where:

U	=	Rotor Tip Speed (ft/sec)
C_0	=	Isentropic Spouting Velocity (ft/sec)
Ψ_N	=	Nozzle Velocity Coefficient
Ψ_R	=	Rotor Velocity Coefficient
ρ	=	Reaction Fraction
α	=	Nozzle Angle
β_3	=	Rotor Exit Blade Angle

The Reynolds Number for Turbines is Defined as:

$$\mathrm{Re} = \frac{D_h \cdot W_2 \cdot \rho_2 \cdot 3600}{\mu_2}$$

Where:

D_h	=	Blade Passage Hydraulic Diameter (ft)
W_2	=	Blade Inlet Relative Velocity (ft/sec)
ρ_2	=	Blade Inlet Density (lb/ft^3)
μ_2	=	Blade Inlet Viscosity (lb/ft-hr)

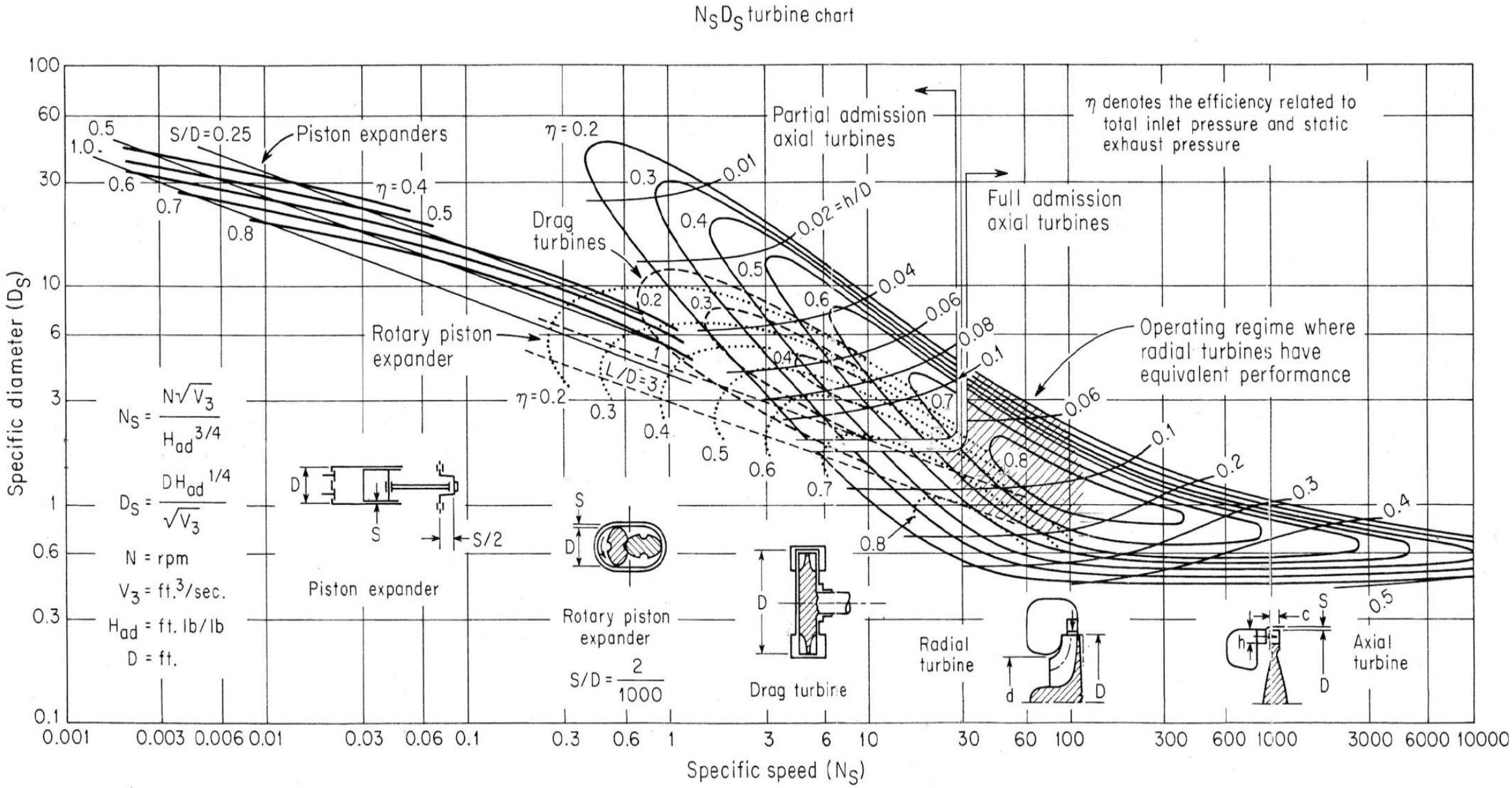
$N_S D_S$ turbine chart
Specific diameter (D_S)
Specific speed (N_S)
100
60
30
10
6
3
1
0.6
0.3
0.1
0.001
0.003
0.006
0.01
0.03
0.06
0.1
0.3
0.6
1
3
6
10
30
60
100
300
600
1000
3000
6000
10000
η denotes the efficiency related to total inlet pressure and static exhaust pressure
Piston expanders
S/D=0.25
0.5
1.0
0.6
0.7
0.8
η=0.4
0.5
Drag turbines
η=0.2
0.3
0.4
0.5
0.6
0.7
0.8
0.01
0.02=h/D
0.04
0.06
0.08
0.1
0.2
0.3
0.4
Partial admission axial turbines
Full admission axial turbines
Rotary piston expander
L/D=3
1
Operating regime where radial turbines have equivalent performance
$N_S = \frac{N\sqrt{V_3}}{H_{ad}^{3/4}}$
$D_S = \frac{D H_{ad}^{1/4}}{\sqrt{V_3}}$
N = rpm
V_3 = ft.^{3}/sec.
H_{ad} = ft. lb/lb
D = ft.
D
S
S/2
Piston expander
Rotary piston expander
$S/D = \frac{2}{1000}$
Drag turbine
Radial turbine
d
Axial turbine
h
c

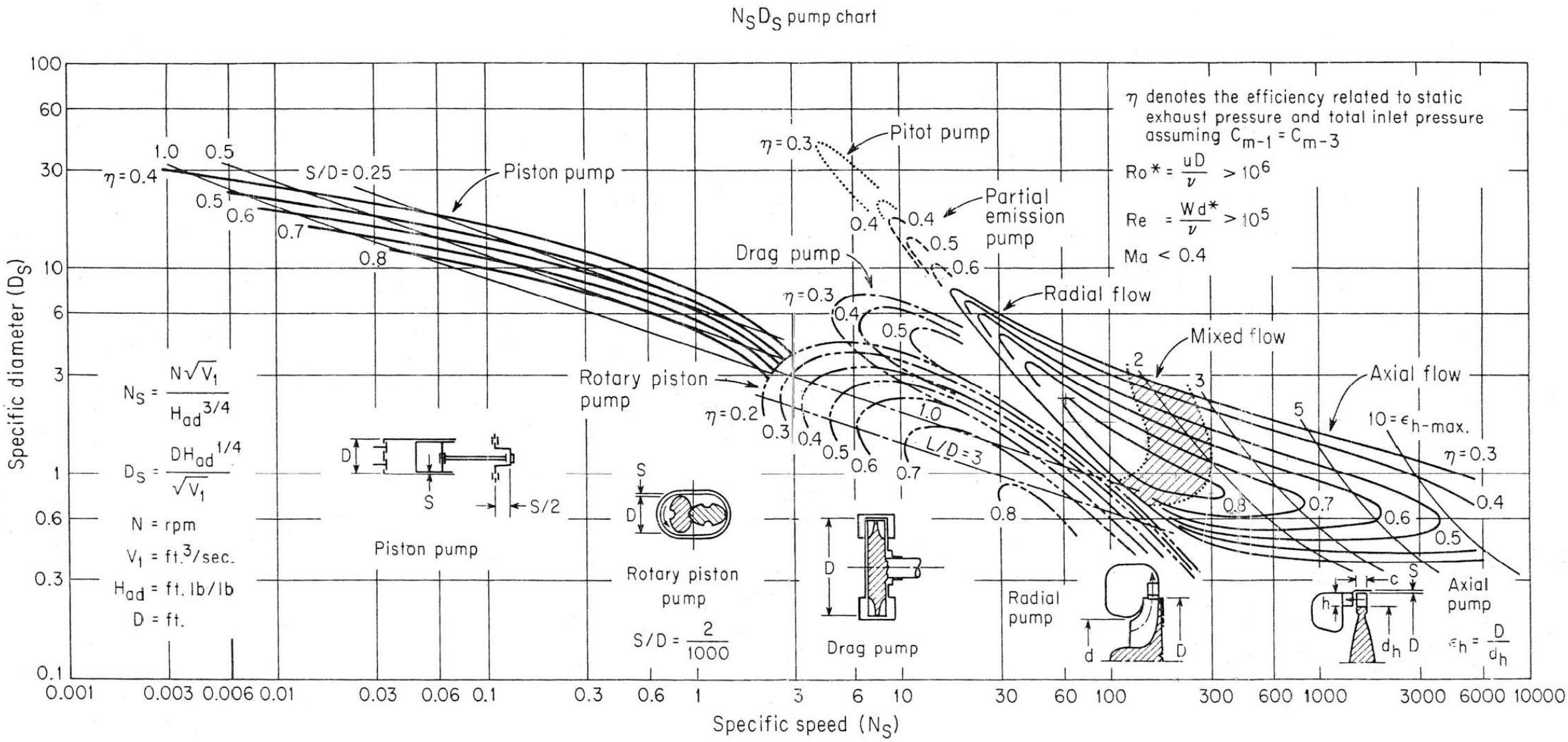
$N_S D_S$ pump chart
Specific diameter (D_S)
Specific speed (N_S)
100
60
30
10
6
3
1
0.6
0.3
0.1
0.001
0.003
0.006
0.01
0.03
0.06
0.1
0.3
0.6
1
3
6
10
30
60
100
300
600
1000
3000
6000
10000
η denotes the efficiency related to static exhaust pressure and total inlet pressure assuming $C_{m-1} = C_{m-3}$
$Ro^* = \frac{uD}{\nu} > 10^6$
$Re = \frac{Wd^*}{\nu} > 10^5$
$Ma < 0.4$
$N_S = \frac{N\sqrt{V_1}}{H_{ad}^{3/4}}$
$D_S = \frac{DH_{ad}^{1/4}}{\sqrt{V_1}}$
N = rpm
V_1 = ft.^{3}/sec.
H_{ad} = ft. lb/lb
D = ft.
Piston pump
S/D = 0.25
0.5
0.6
0.7
0.8
1.0
η = 0.4
Pitot pump
η = 0.3
0.4
Partial emission pump
0.5
0.6
Drag pump
η = 0.3
0.4
0.5
Radial flow
Mixed flow
Axial flow
Rotary piston pump
η = 0.2
0.3
0.4
0.5
0.6
0.7
1.0
L/D = 3
0.8
2
3
5
10 = $\epsilon_{h\text{-max.}}$
η = 0.3
0.4
0.5
0.6
0.7
0.8
D
S
S/2
Piston pump
S
D
Rotary piston pump
$S/D = \frac{2}{1000}$
D
Drag pump
Radial pump
d
D
c
S
h
d_h
D
Axial pump
$\epsilon_h = \frac{D}{d_h}$

A single wellbore geothermal energy conversion system using downhole heat exchanger with zero mass withdrawal concept

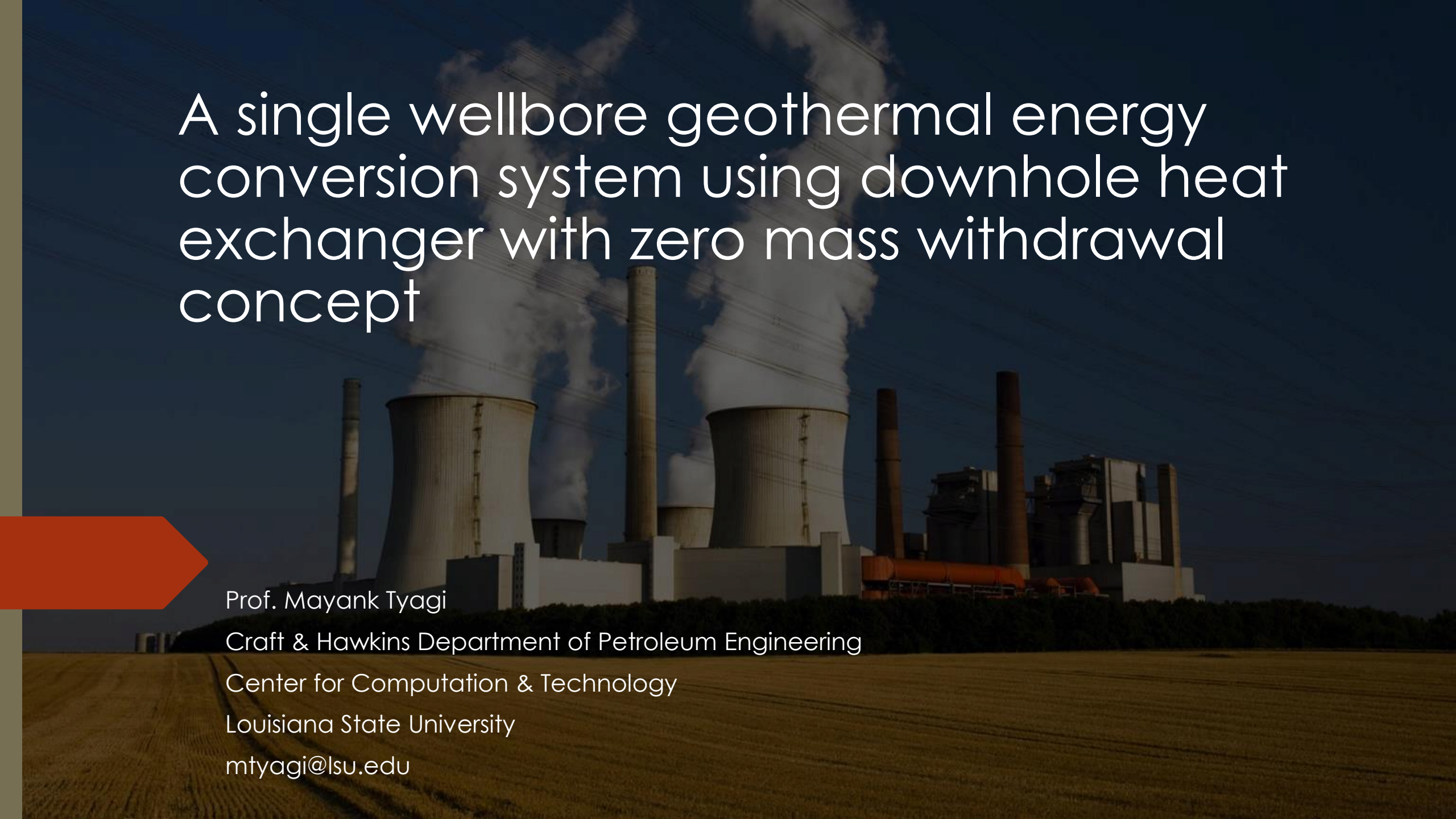

Prof. Mayank Tyagi
Craft & Hawkins Department of Petroleum Engineering
Center for Computation & Technology
Louisiana State University
mtyagi@lsu.edu

Motivation

PROCEEDINGS, Thirty-Eighth Workshop on Geothermal Reservoir Engineering
Stanford University, Stanford, California, February 11-13, 2013
SGP-TR-198

GEOTHERMAL ENERGY: THE ENERGY-WATER NEXUS

Christopher Harto, Jenna Schroeder, Lou Martino, Robert Horner and Corrie Clark

to wet or hybrid systems; however they come at a cost of an energy penalty that increases when power is the most valuable in the summer. Flash plants typically use condensate to run wet cooling systems, however this comes at a cost of reduced reservoir sustainability. Supplemental injection programs can extend the life of the reservoir but consume large quantities of water relative to other electric generation technologies. The large resource base for enhanced geothermal systems (EGS) represents a major opportunity for the geothermal industry; however, depending upon geology, these systems can be quite "thirsty" and require large quantities of make-up water due to below ground reservoir losses. Identifying potential sources of compatible degraded or low quality water for use for make-up injection for EGS and flash systems represents an important opportunity to reduce the impacts of geothermal development on fresh water resources. The importance of identifying alternative water sources for geothermal systems is heightened by the fact that a large fraction of the geothermal resource is located in areas already experiencing water stress.

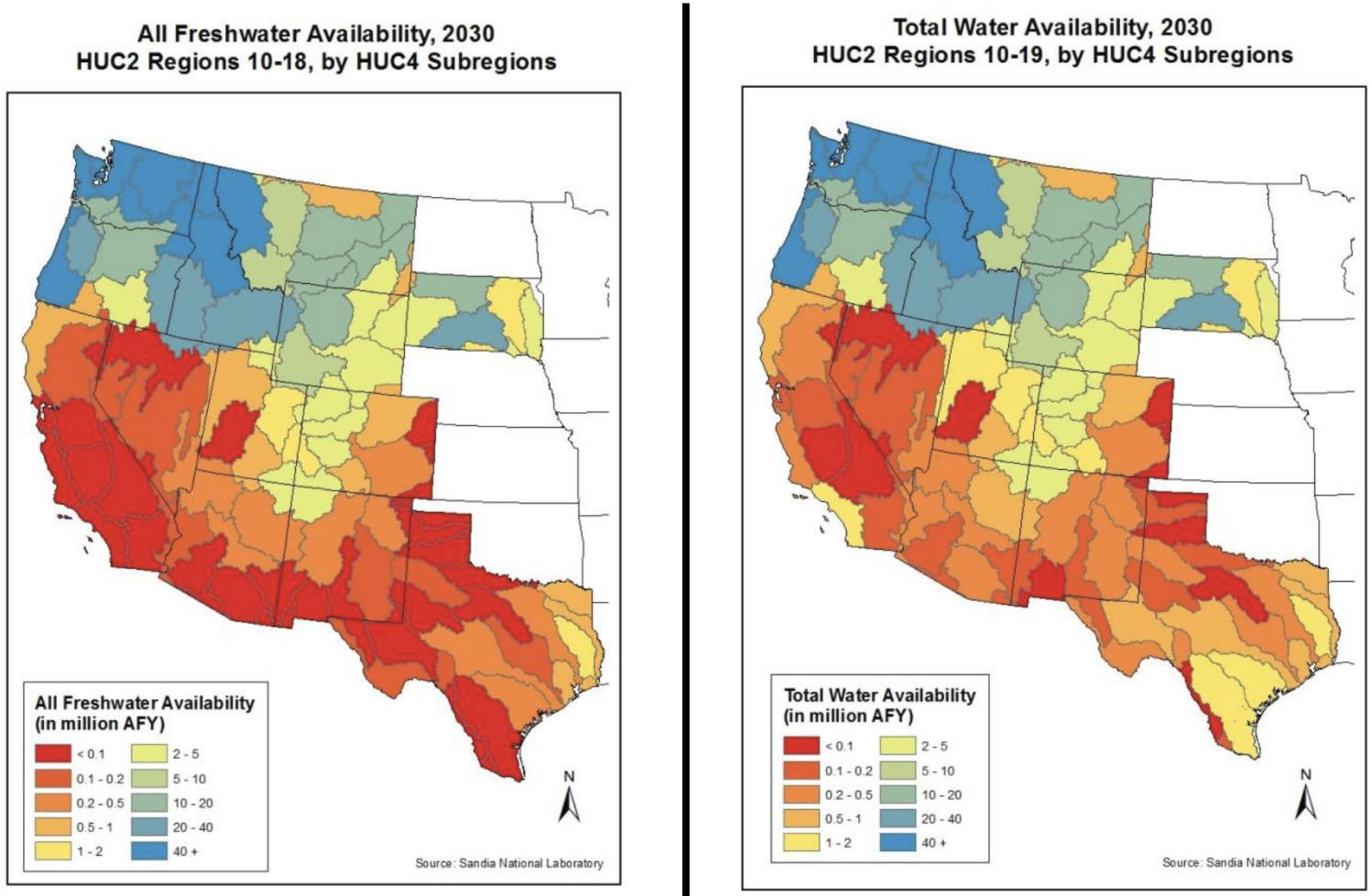

Figure 3: Water Availability Metrics Developed by Sandia National Laboratories (Source: Tidwell 2012): Freshwater Availability (left) and Total Water Availability (right)

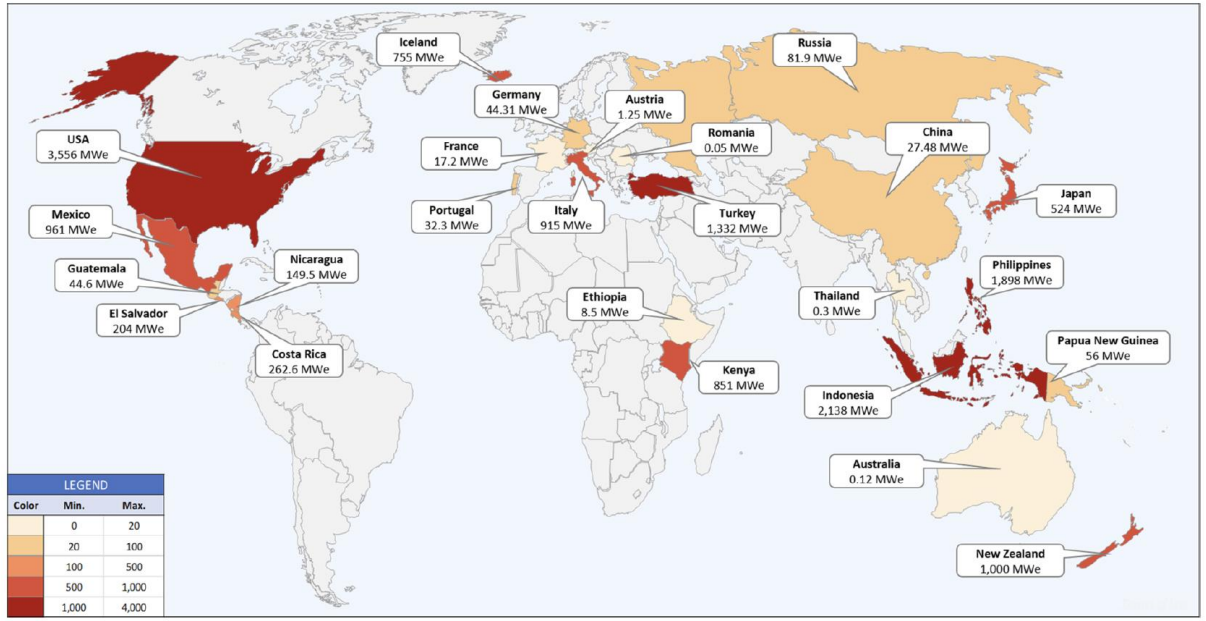

Fig. 2. Global geothermal installed capacity map, based on published data (Appendix A–F) at the point of preparing this work (early 2020) (created by using Someka Excel Generator (2019)).

Reinjection in geothermal fields: An updated worldwide review 2020

Zahratul Kamila, Eylem Kaya *, Sadiq J. Zarrouk

Department of Engineering Science, University of Auckland, Private Bag 92019, New Zealand

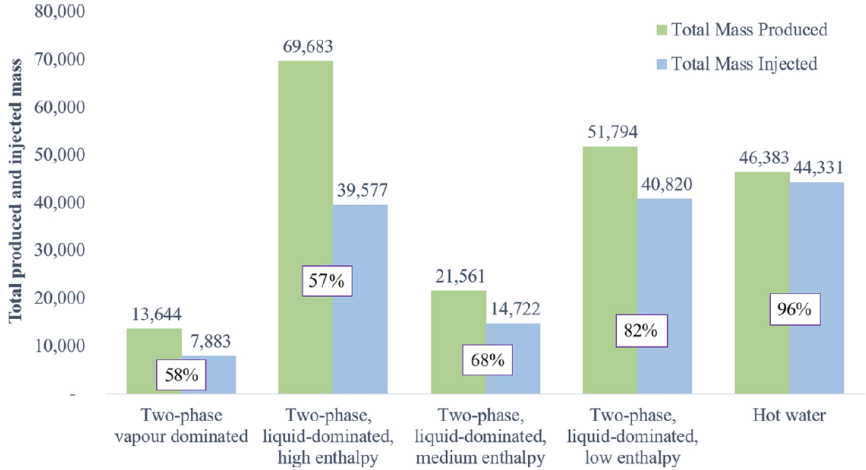

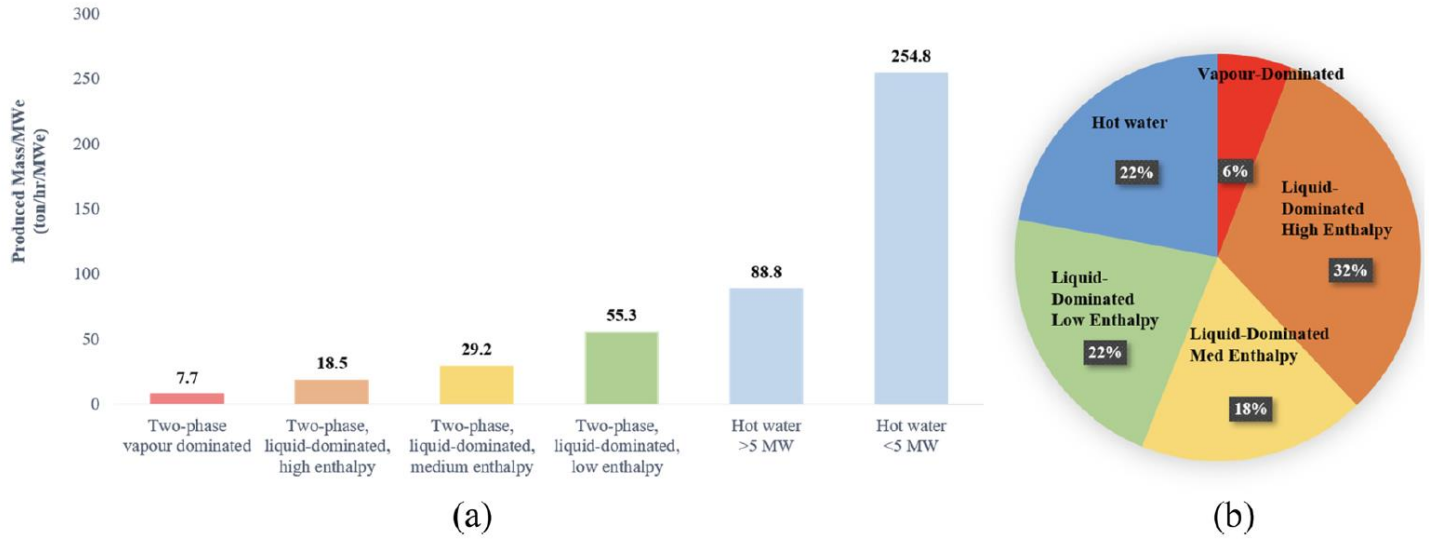

Fig. 5. (a) Produced mass (t/h) per MWe for each type of geothermal system (b) total produced mass per type of system based on published data (Appendix A-F).

Risks:

Chemical/Thermal Breakthrough
Cooling
Injectivity
Scales/Solids
Micro-seismicity
Surface deformation (Subsidence/Lifting)

Background

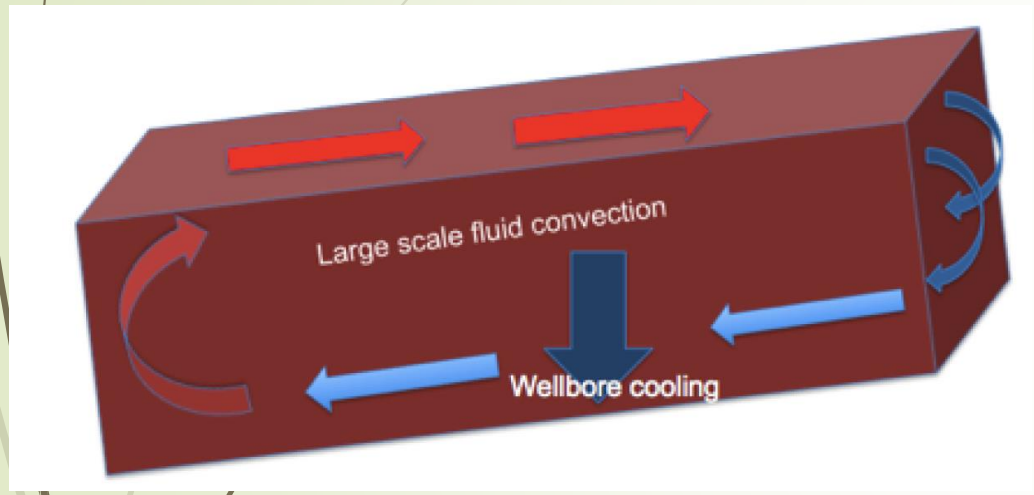

2011

Modeling effects of coupled convection and CO2 injection in stimulating geopressured geothermal reservoirs

Tatyana Plaksina
Louisiana State University and Agricultural and Mechanical College

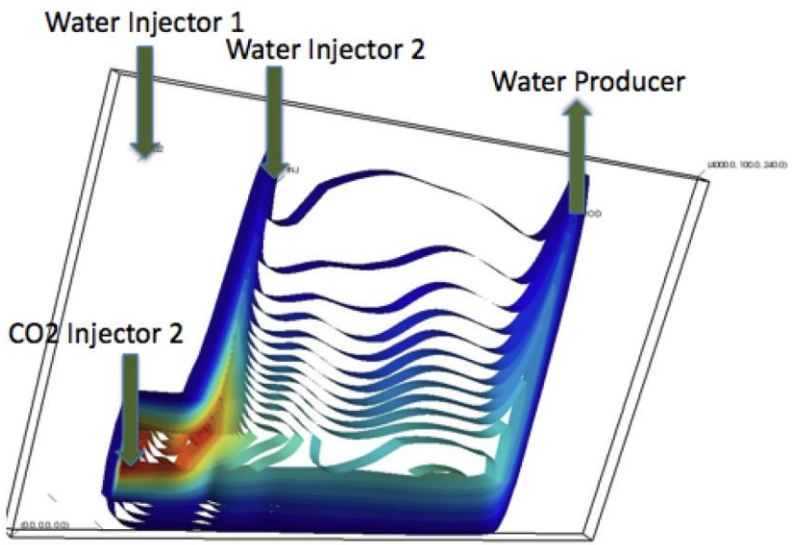

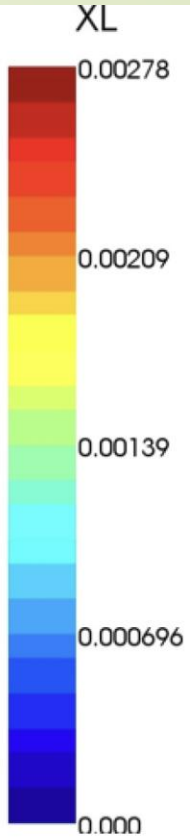

Figure 6.8: CO_2 injection with heat extraction and an additional dynamic control well 1. Snapshot of liquid CO_2 mass fraction is taken after 30 years of injection. The supercritical gas mixes with geolfuid faster. This leads to lower gas concentration and prevents formation of the plume. The reservoir is a 2D geomodel with length of 4000 m, width of 100 m, and height of 200 m (with 10-fold exaggeration in z-direction). Permeability is 1 D and porosity is 0.2. Gas injection rate is 0.003 kg/s. The plot's legend represents mass fraction of liquid CO_2 (no gas phase).

DOE-GTP Project

Supported 4 PhDs and 1 MS. Project built upon the initial research ideas presented in 1 MS (Plaxina) and 1 PhD (Feng).

DE-EE0005125
Louisiana State University
FY2016, Final

Final Research Performance Progress Report

Federal Agency and Organization: DOE EERE – Geothermal Technologies Program

Recipient Organization: Louisiana State University and A&M College
DUNS Number: 075050765
Recipient Address: Patricia M. Territo, Director
Sponsored Program Accounting Office
Louisiana State University and A & M College
336 Thomas Boyd Hall
Baton Rouge, Louisiana 70803-2901

Award Number: DE-EE0005125
Project Title: Geothermal Resource Development with Zero Mass Withdrawal, Engineered Convection, and Wellbore Energy Conversion
Project Period: 9/1/2011-9/30/2016

Scope of this talk

Geothermics 53 (2015)

A downhole heat exchanger for horizontal wells in low-enthalpy geopressured geothermal brine reservoirs

Yin Feng [1], Mayank Tyagi [*], Christopher D. White [2]

Craft & Hawkins Department of Petroleum Engineering, Louisiana State University, United States

Geothermal Energy 5:13 (2017)

Numerical analysis of downhole heat exchanger designed for geothermal energy production

I. Akhmadullin* and M. Tyagi

De-risking Geothermal Energy Extraction and Conversion

- Single Directional Wellbore (=> Cost)
- Zero Mass Withdrawal (ZMW) (=> Surface handling and reinjection cost)
- Long Downhole Heat Exchanger (=> Improved efficiency)
- Reduced risks for microseismicity, subsidence, or lifting (=> Lower maintenance cost)
- Maintain wellbore integrity (=> Closer to reservoir TE during operational life)
- Potential for within wellbore energy conversion (=> Critical Infrastructure)
- Potential to combine with "OTHER" metrics (=> Economics and Sustainability)

ZMW Concept

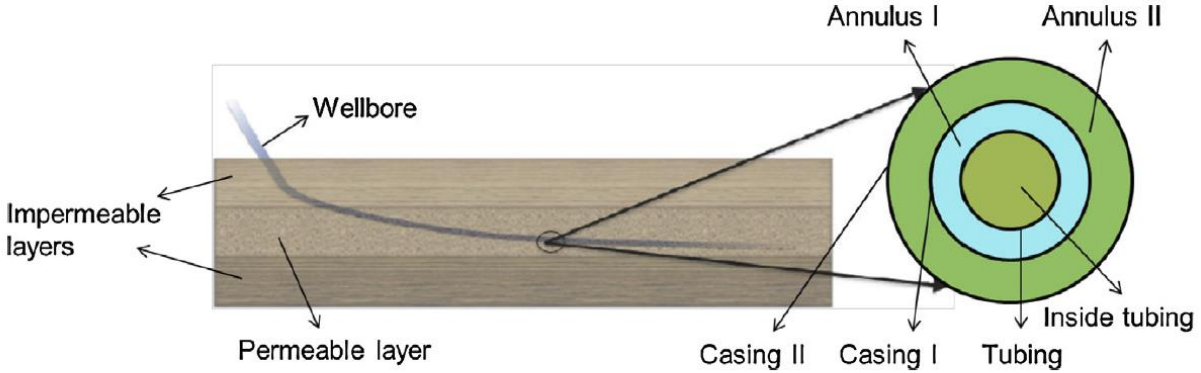

Fig. 1. Schematic of wellbore paths and DHE cross-section (Tyagi and White, 2010).

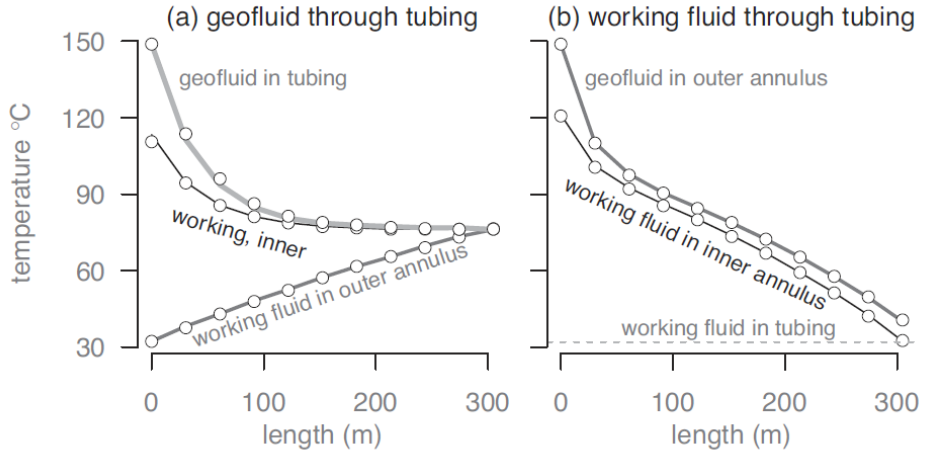

Fig. 4. Temperature variation along flow path in the DHE for different configurations [lines: analytical solution; symbols: numerical solution].

Table 1
Baseline parameters for sensitivity study.

Reservoir properties	
Rock density	2700 kg m^{-3}
Heat conductivity	1.9 W m^{-1}K^{-1}
Temperature	149 °C
DHE geometry	
Length (baseline)	305 m
Outer casing OD, ID	21.91, 19.37 cm
Inner casing OD, ID	16.83, 15.36 cm
Tubing OD, ID	12.70, 10.86 cm
Heat conductivity	45 W m^{-1}K^{-1}
Working fluid (n-butane) properties	
Density	582 kg m^{-3}
Heat conductivity	0.107 W m^{-1}K^{-1}
Specific thermal capacity	2763 J kg^{-1} K^{-1}
Viscosity	1.7×10^{-4} Pa s
Injection temperature	32 °C
Mass flow rate	5.25 kg s^{-1}
Geofluid (water) properties	
Density	1000 kg m^{-3}
Heat conductivity	0.519 W m^{-1}K^{-1}
Specific thermal capacity	3182 J kg^{-1} K^{-1}
Viscosity	1.1×10^{-4} Pa s
Mass flow rate	2.34 kg s^{-1}

Results

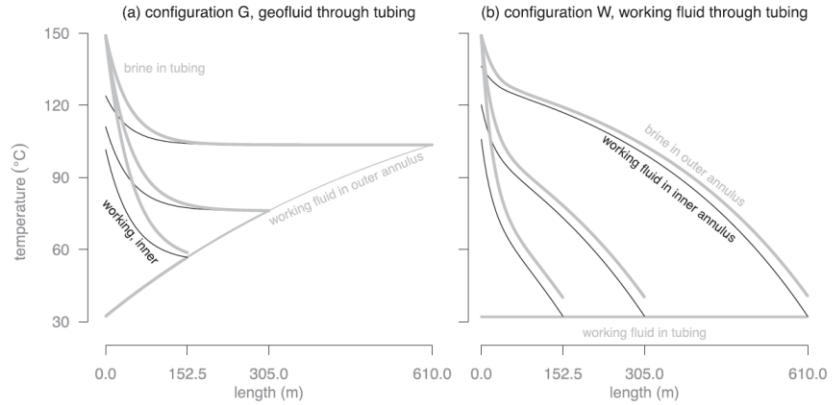

Fig. 5. Temperature variation for three heat exchanger lengths. (a) For configuration *G*, the working fluid is warmed in the annulus by convection. For longer DHE lengths, further heating of the working fluid occurs only near the brine inlet near the heel of the well. (b) For configuration *W*, the tubing is insulated so that there is no warming of the working fluid until it reaches the toe of the well and reverses into the inner annulus.

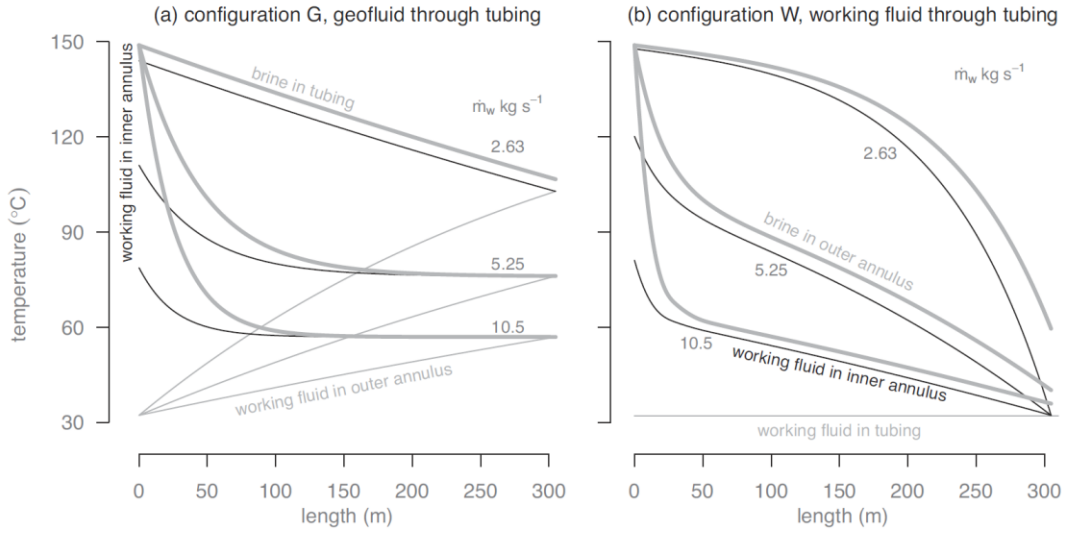

Fig. 6. Temperature variation for three working fluid mass flow rates [10.5, 5.25 and 2.63 kg s^{-1}].

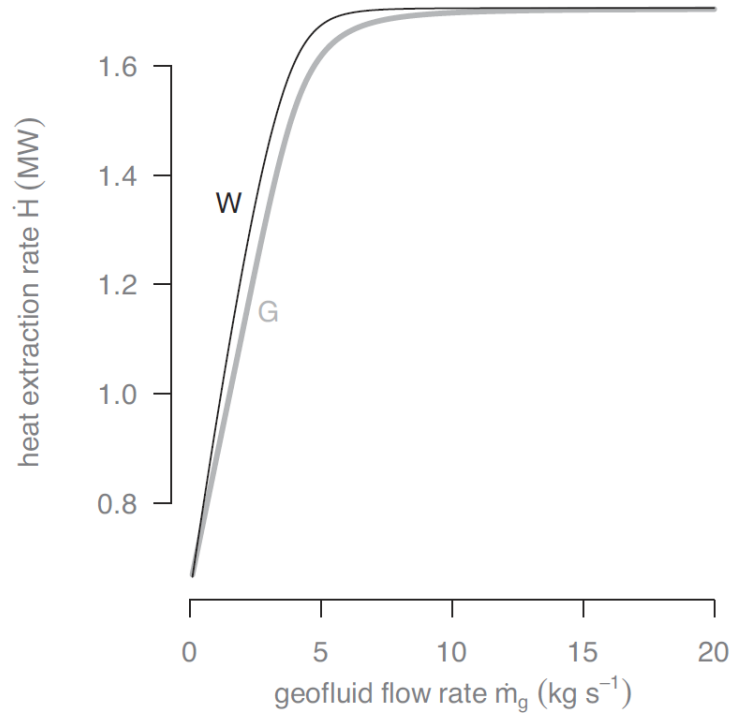

Fig. 9. Variation of rate of enthalpy extraction for varying woking fluid rates. At low working fluid rates, performance is identical, as both configurations heat the working fluid to very near the reservoir temperature and the extracted enthalpy varies linearly with the working fluid rate. The working fluid through the tubing (*W*) configuration performs slightly better in the transition range, until both systems plateau for rates greater than ca. 20 kg s^{-1}.

Field Case Study

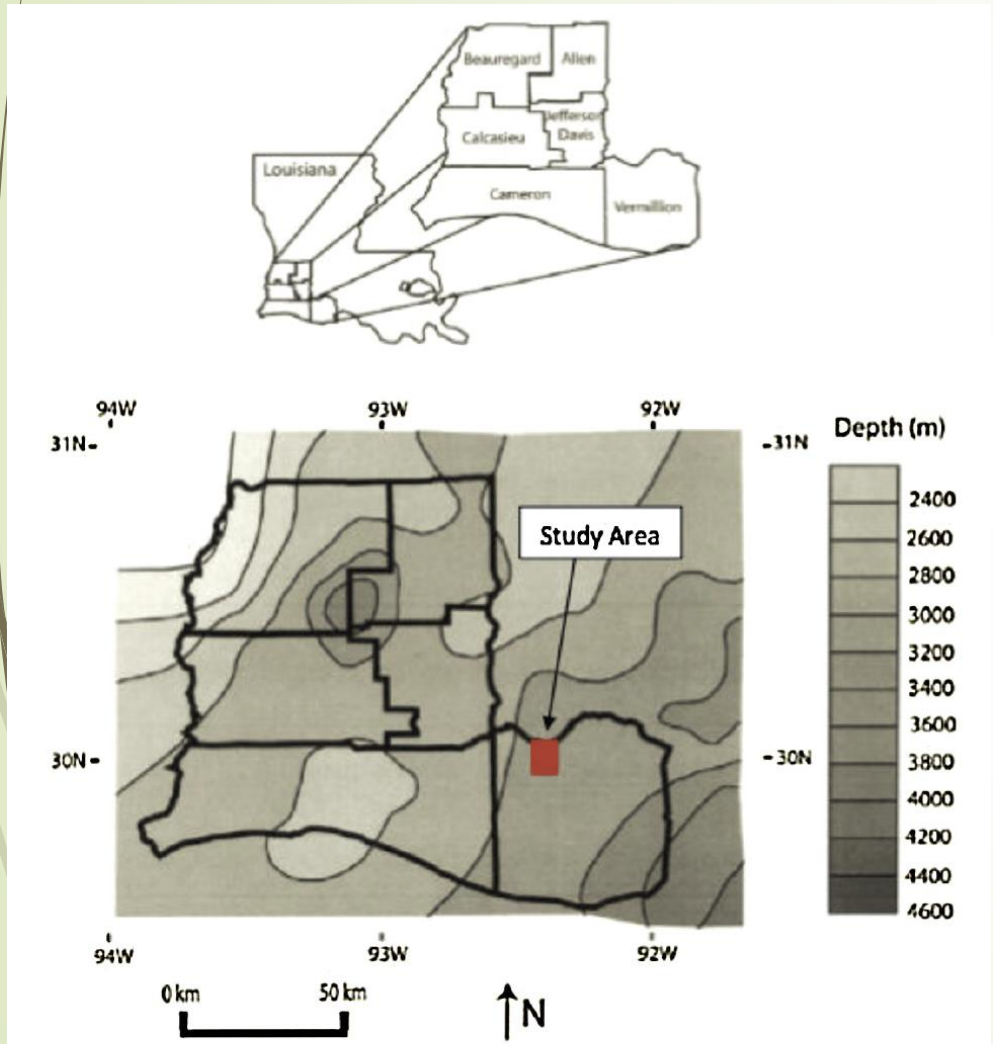

Fig. 11. 100 °C isotherm map of the study area (Szalkowski and Hanor, 2003).

Parameters for the computational model.

Reservoir	
Rock density	2700 kg m^{-3}
Heat conductivity	1.9 W m^{-1} °C
Geothermal gradient	28 °C km^{-1}
Permeability	200 mD
Porosity	0.20
Dip angle	5°
Thickness	100 m
Width × length	2000 m × 2000 m
Geofluid	
Density	1000 kg m^{-3}
Heat conductivity	0.649 W m^{-1} °C^{-1}
Specific thermal capacity	3726 J kg^{-1} °C^{-1}
Viscosity	3 × 10^{-4} Pa s

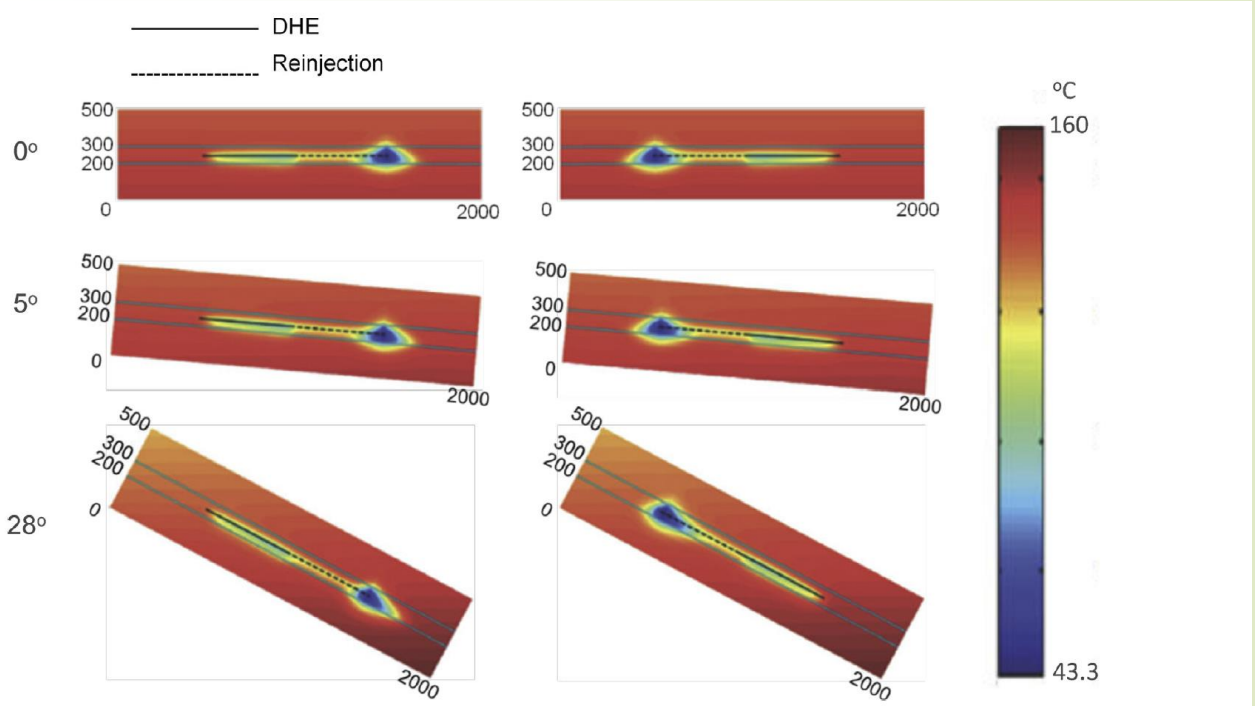

Fig. 16. Temperature contours of the 2D x–z plane in the middle of the 3D system (y = 1000 m) containing the DHE [top: 0°; middle: 5°; bottom: 28° and left: down dip; right: up dip], where the solid line represents the DHE section and the geofluid is reinjected through dash line further away.

Design - Subsystems

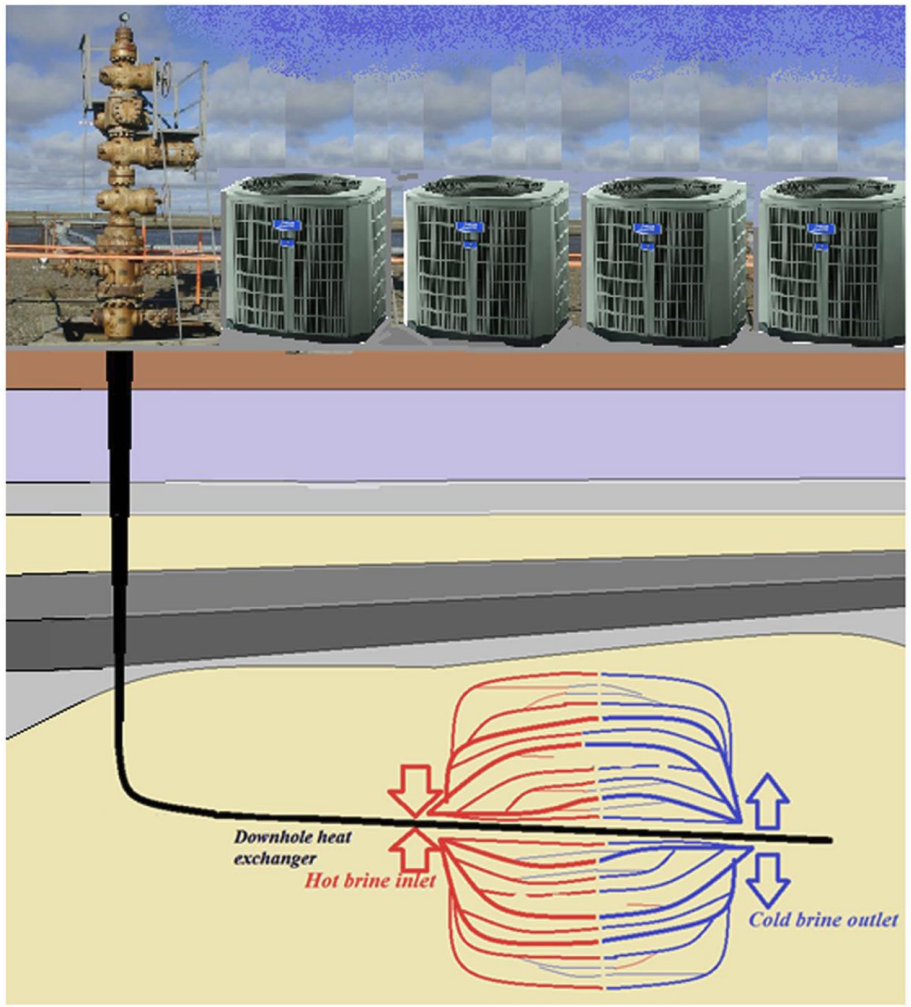

Fig. 1 Zero mass withdrawal method scheme

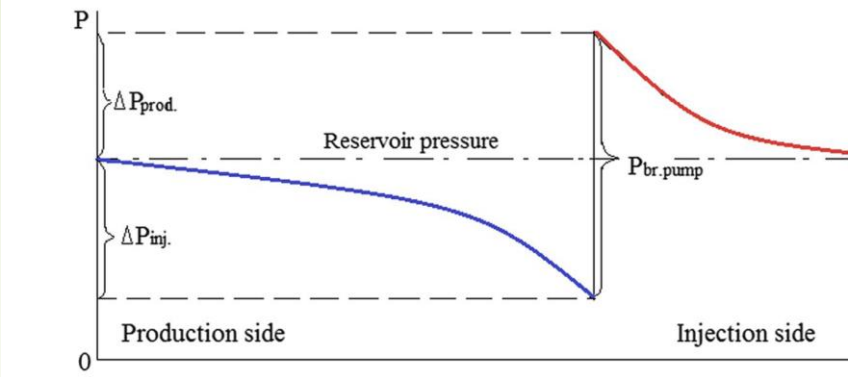

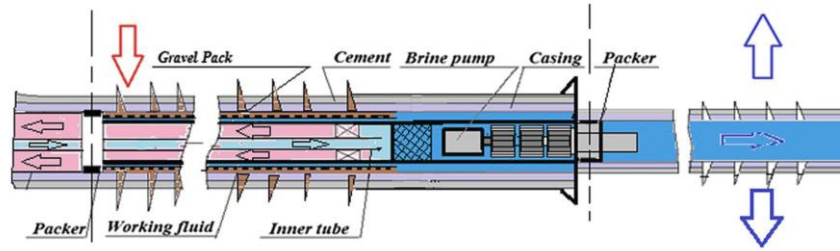

Fig. 4 Pressure distribution along the well

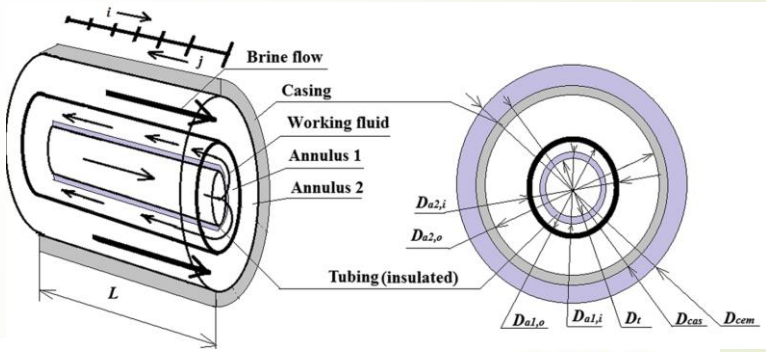

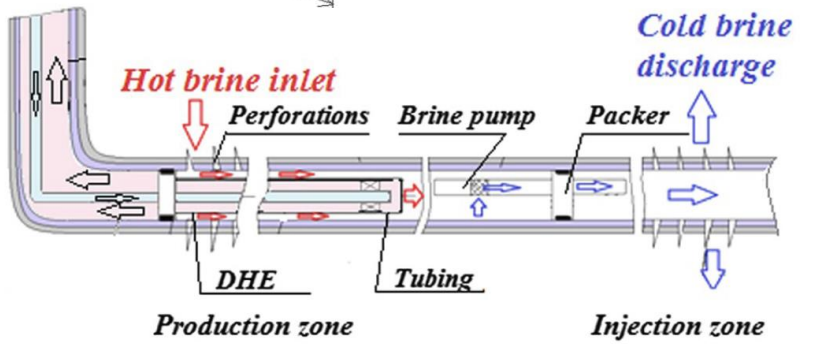

Completion design scheme for a horizontal well with the downhole heat exchanger

Operational principle - Zero Mass Withdrawal (ZMW)

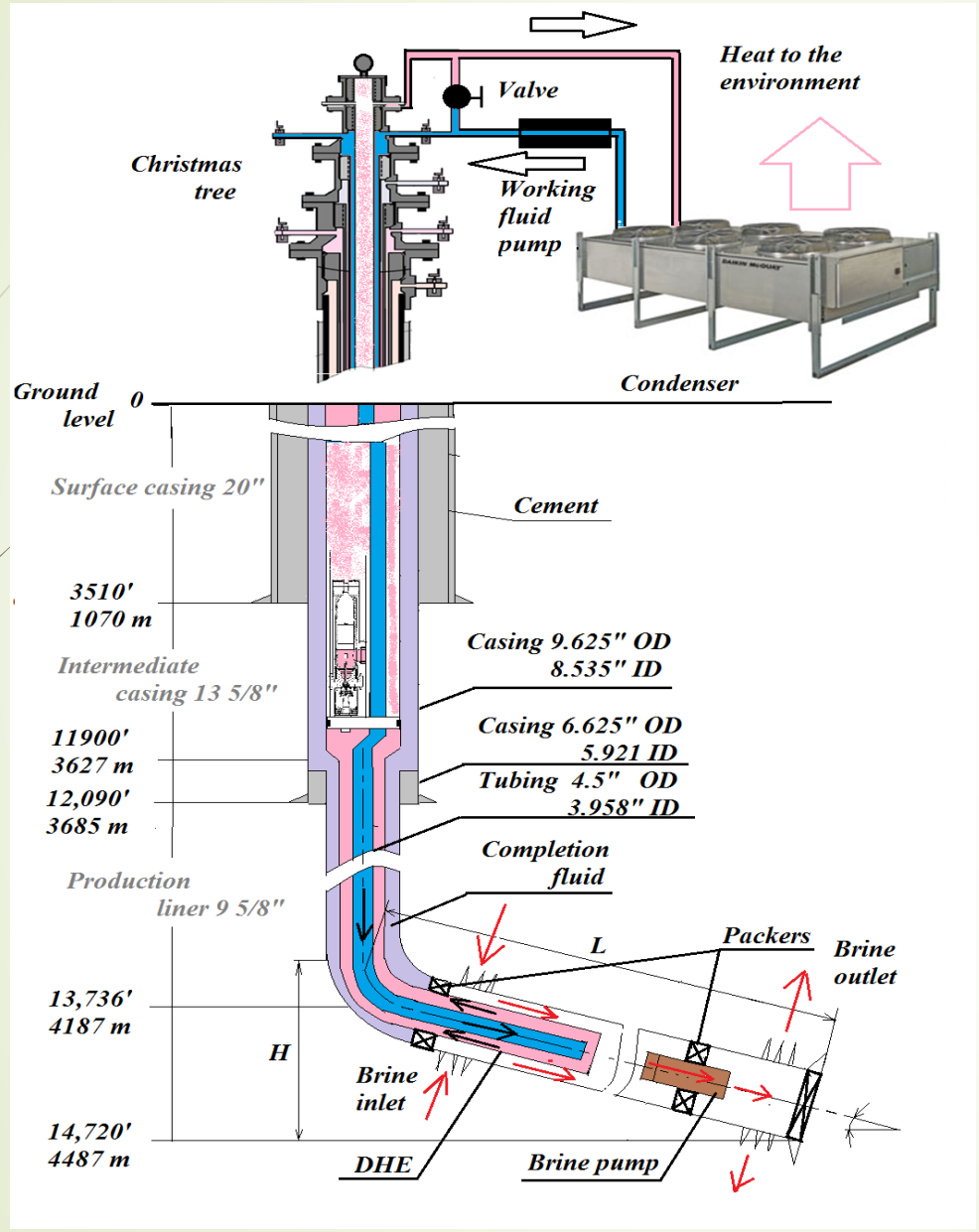

Heat Rejection Subsystem

Power Generation Subsystem

Heat Extraction Subsystem

The schematic was designed for the reference reservoir conditions

Working Fluids Selection

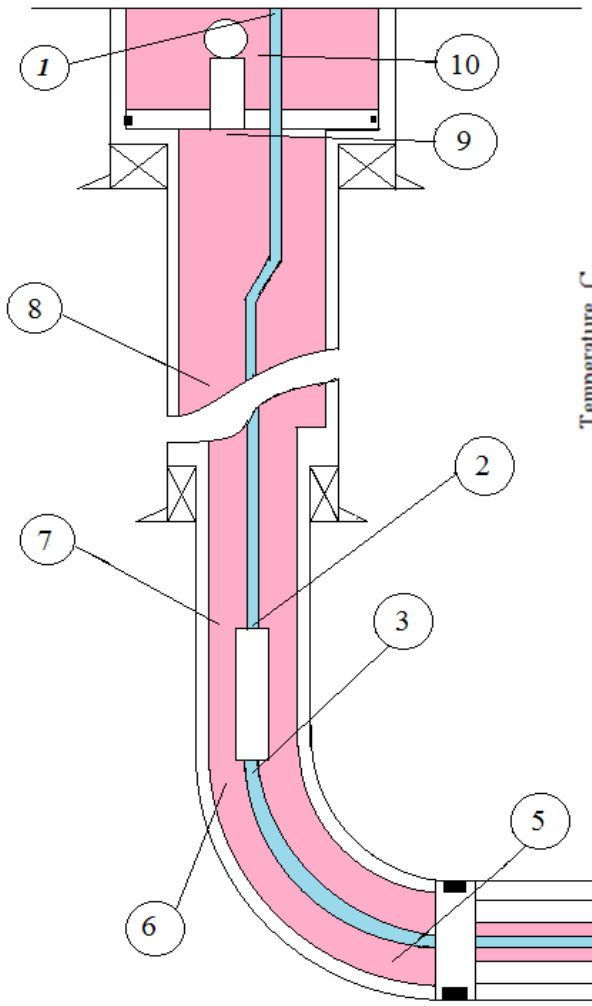

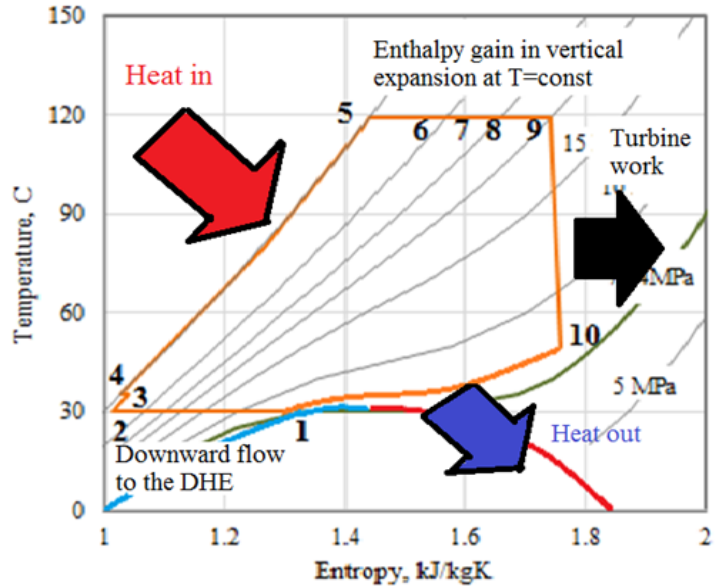

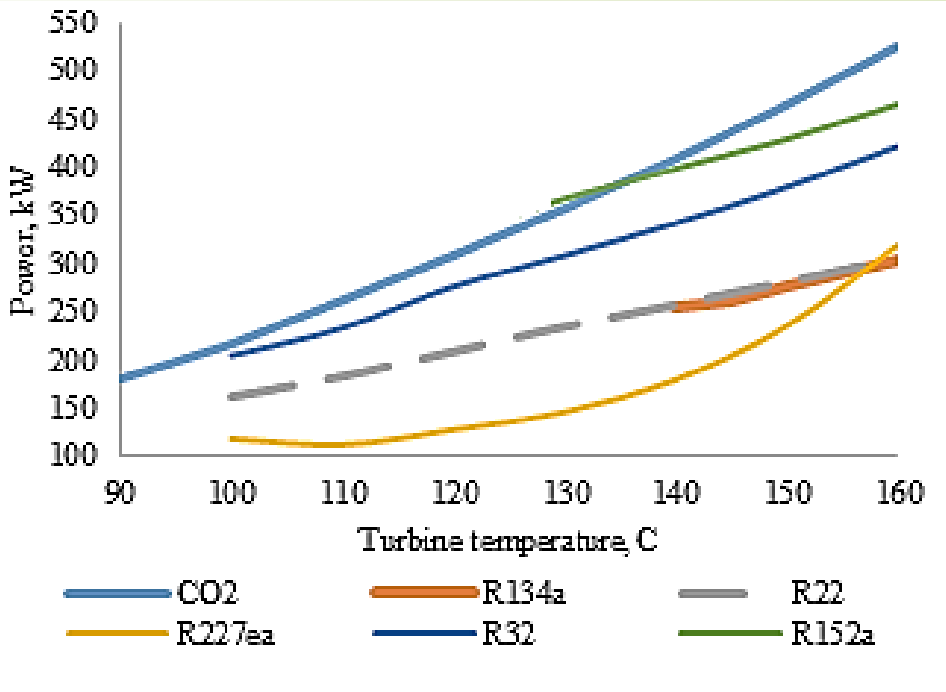

Turbine power production with different working fluids

Power extraction subsystem

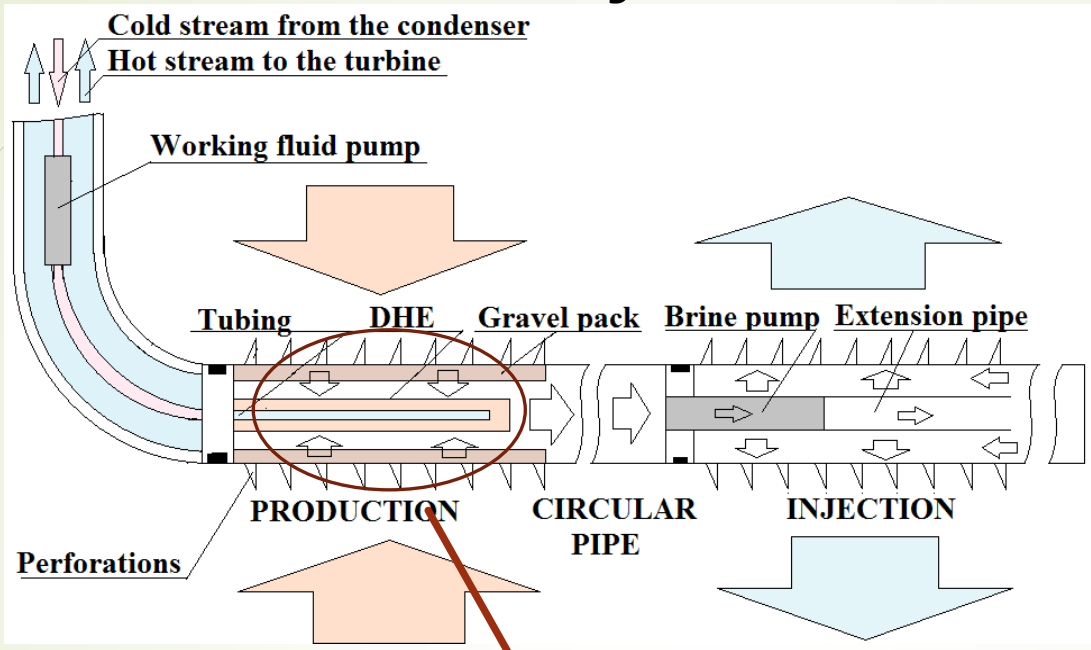

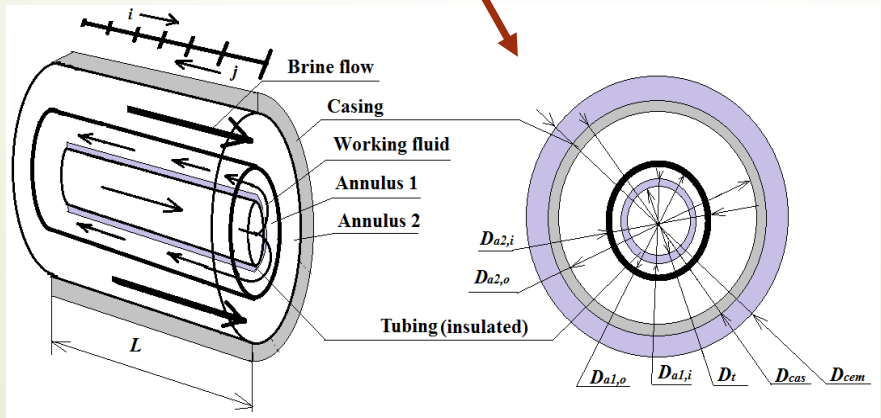

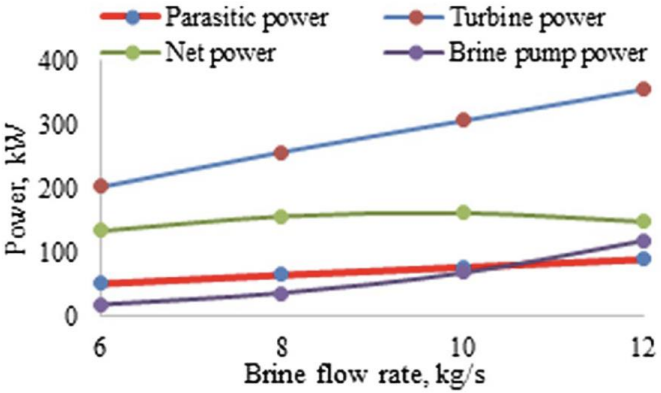

Net power development vs brine flow rate

LCOE

Reservoir temperature 126C

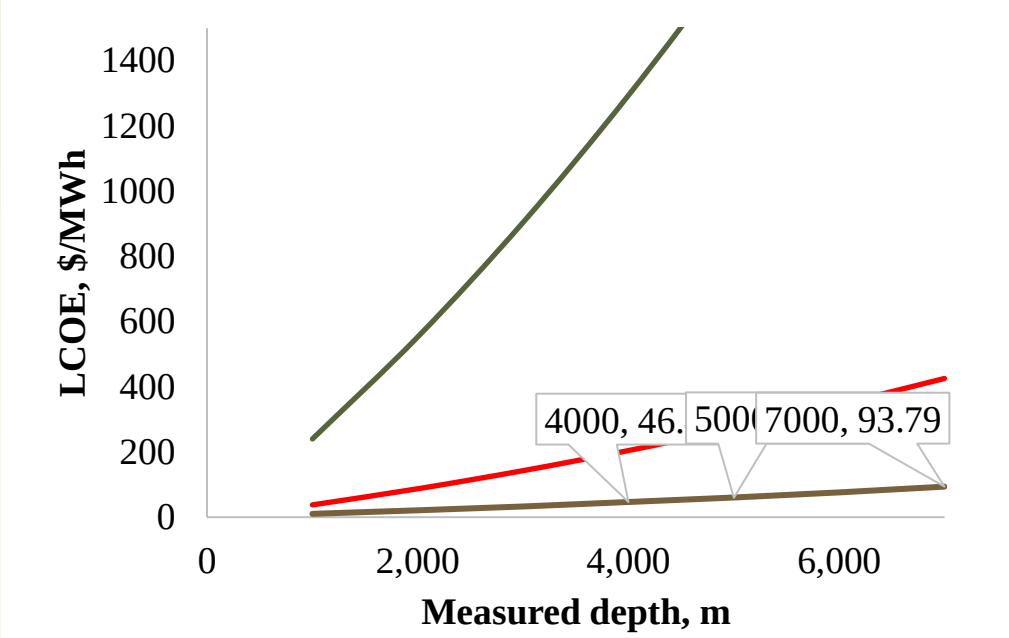

Power Plant Type	Cost ($/kWh)
Coal	$0.12
Natural Gas	$0.10
Nuclear	$0.10
Wind	$0.08 - $0.20
Solar PV	$0.13
Solar Thermal	$0.24
Geothermal	$0.05
Biomass	$0.10
Hydro	$0.08

Reservoir temperature 220C

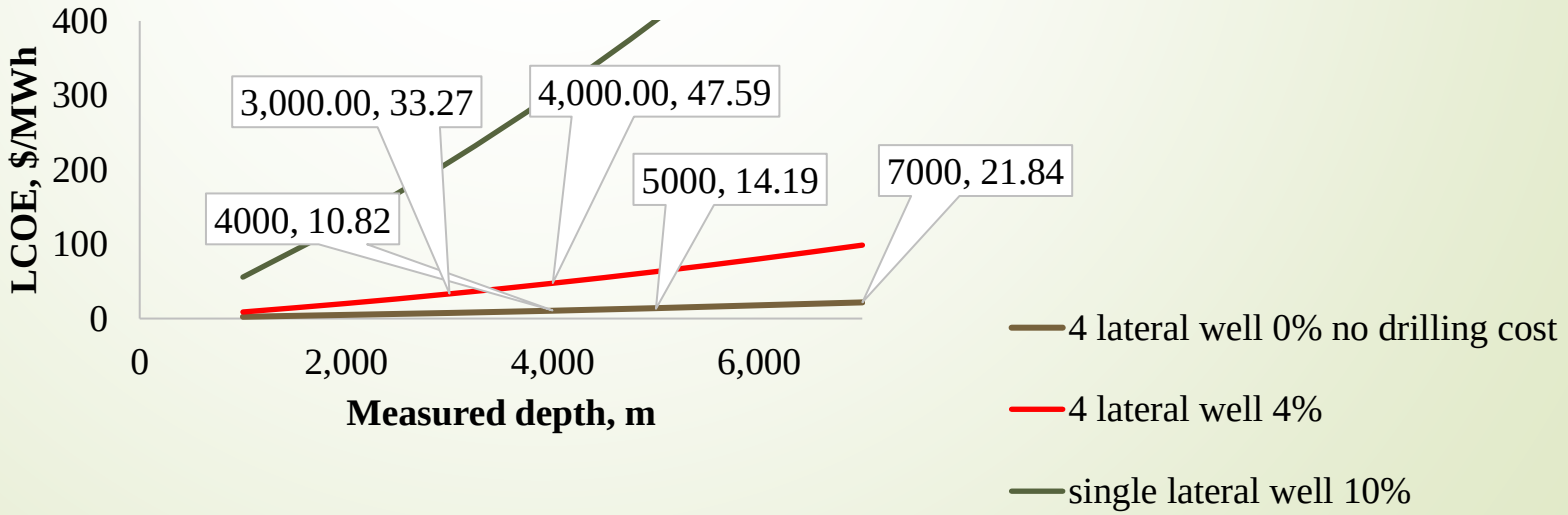

References

- Akhmadullin, I., Design and Analysis of Low-Enthalpy Geothermal Wellbore Energy Conversion System Working on Zero Mass Withdrawal Method, PhD Dissertation, LSU, (2016)
- Bejan A., Second-law analysis in heat transfer and thermal design. in:T.F. Irvine, J.P. Hartnett (Eds.), Advance in Heat Transfer, vol. 15. Elsevier, NewYork, 1982, pp. 1e58.
- Bianchi M., De Pascale A., Bottoming cycles for electric energy generation: Parametric investigation of available and innovative solutions for the exploitation of low and medium temperature heat sources, Applied Energy, (2011)
- Bridger D.W and Allen D.A, Designing Aquifer Thermal Energy Storage Systems, ASHRAE Journal, Vol. 47, No. 9, (2005)
- DiPippo R., Second Law assessment of binary plants generating power from low-temperature geothermal fluids, Geothermics 33, (2004)
- El-Sayed A-A.H., Khalaf F., Ghzaly S.M., Casing Design Considerations for Horizontal Wells, SPE 21386, (1991)
- Feng Y., Numerical Study of Downhole Heat Exchanger Concept in Geothermal Energy Extraction From saturated and Fractured Reservoirs, PhD Dissertation, LSU, (2012)
- Gray T.A., Geothermal Resource Assessment of the Gueydan Salt Dome and the Adjacent South-East Gueydan Field", Vermilion Parish, Louisiana, Master Thesis, LSU, (2010)
- Moran M.J., Shapiro H.N, Fundamentals of Engineering Thermodynamics, 6-th edition, John Wiley and Sons, Inc, (2008)


Q&A

- Nathenson, M. Physical factors determining the fraction of stored energy recoverable from hydrothermal convection systems and conduction-dominated areas, USGS-OFR-75-525.
- Jurado, N.R. Thermal performance evaluations of fractured and closed-loop geothermal reservoirs, MS Thesis, Cornell University, 2021.
- Rybach, L., Megel, T., Eugster, W.J. At what time scale are geothermal resources renewable? Proc. World Geothermal Congress, Japan, 2000.
- Gao, J., Shi, Q. A new mathematical modeling approach for thermal exploration efficiency under different geothermal well layout conditions, Scientific reports (2021) 11:22930.

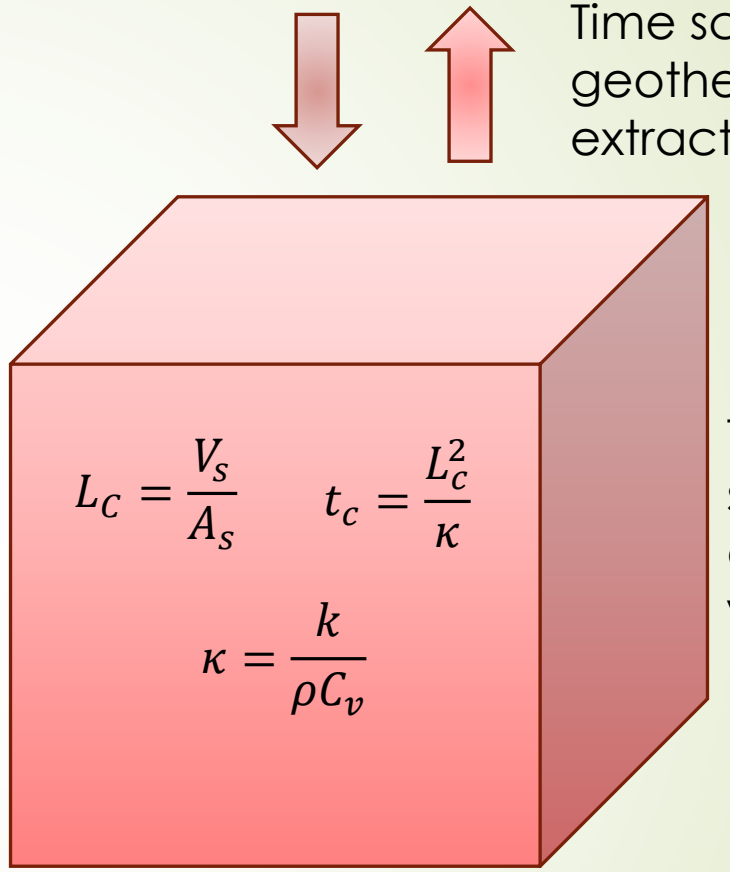

Time scales for geothermal heat extraction operations

$$L_C = \frac{V_s}{A_s} \qquad t_c = \frac{L_c^2}{\kappa}$$

$$\kappa = \frac{k}{\rho C_v}$$

Time scales for storage/depletion of heat in working/geofluids

$$\text{Bi} = \frac{hL_c}{k}$$

$$\text{Nu} = \frac{hL_c}{k}$$

$$Gr = \frac{g\beta\left(T_R - T_f\right)L_c^3}{\nu^2}$$

Time scales for geological recharge mechanism of geothermal heat